Luminance Degradation Compensation Based on Multi-Stream Self-Attention to Address Thin Film Transistor-Organic Light Emitting Diode Burn-in

Seongchel Park, **Kwan-Ho Park** and **Joon-Hyuk Chang** *

Department of Electronics and Computer Engineering, Hanyang University, Seoul 04763, Korea; psc0902@hanyang.ac.kr (S. P.); rhksgh7370@naver.com (K.-H. P.)
* Correspondence: jchang@hanyang.ac.kr; Tel.: +82-2-2220-0355

Abstract: We propose a deep learning algorithm that directly compensates for luminance degradation owing to the deterioration of organic light emitting diode (OLED) devices to address the burn-in phenomenon of OLED displays. Conventional compensation circuits are encumbered by a high cost of development and manufacturing processes owing to their complexity. However, given that deep learning algorithms are typically mounted on a system on chip (SoC), the complexity of the circuit design is reduced, and the circuit can be reused by re-learning only the changed characteristics of the new pixel device. The proposed approach comprises deep feature generation and multi-stream self-attention, which decipher the importance of the variables, and the correlation between burn-in-related variables. It also utilizes a deep neural network that identifies the nonlinear relationship between the extracted features and luminance degradation. Thereafter, the luminance degradation is estimated from the burn-in-related variables, and the burn-in phenomenon can be addressed by compensating for the luminance degradation. The experimental results revealed that compensation was successfully achieved within an error range of 4.56%, and demonstrate the potential of a new approach that can mitigate the burn-in phenomenon by directly compensating for pixel-level luminance deviation.

Keywords: thin film transistor (TFT); organic light emitting diode (OLED); compensation circuit; luminance degradation; artificial intelligence; deep neural network; convolutional neural networks

1. Introduction

Currently, two types of displays are widely used. The first is the liquid crystal display (LCD), which generates images by controlling the amount of light emitted by the backlight unit (BLU). The second is an organic light emitting diode (OLED), which generates an image by controlling the amount of current supplied to the OLED device. OLED displays have significant advantages such as high color reproduction ranges, low power consumption, high brightness, high contrast ratio and wide viewing angle [1–3]. However, despite their excellent performance, they are hindered by the burn-in phenomenon. This phenomenon is caused by the operating mechanism of OLED displays. Its panels are composed of thin film transistor (TFT)-OLED devices mounted on each pixel, and they function as follows. First, a voltage is applied to the TFT device. Second, the TFT device controls the amount of current supplied to the OLED element according to the applied voltage. Finally, the OLED device controls the brightness of the display by adjusting the luminance according to the supplied current. In this operation, the OLED device is exposed to high temperatures owing to its luminescence characteristics. If this situation persists, it leads to problems with the driving voltage deviation of the TFT device and luminance deviation of the OLED device. Eventually, as the usage time increases, the deterioration of the OLED device accelerates, and luminance degradation occurs [4,5]. Indeed, Xia et al. [6] introduced that OLED luminance degradations is caused by intrinsic and/or extrinsic factors. Intrinsic factors are generally related to moisture or oxygen. Those can be the

cause of delamination or oxidation of the electrodes. Extrinsic factors are related to the degradation of supply voltage-current and the change of ambient temperature during the whole lifetime of OLED displays [7,8]. In addition, Kim et al. [9] showed that the characteristic of color and luminance degradation. They used an electroluminescence (EL) degradation model of R, G, and B pixel over stress time, and obtained that the blue pixel degrades faster than other pixels. They also described that the luminance degradation tends to decrease rapidly at the beginning of use, then become more gradual. Some several studies showed the power consumption for R, G, and B components of an OLED pixel by power models. The blue color consumes more power as compared to the red and green color components [10–12]. Ultimately, the burn-in phenomenon is a major cause of the deterioration of the image and video quality over time [13–16]. Therefore, research on pixel compensation technology that effectively addresses the burn-in phenomenon of OLED displays is important to continuously provide high-quality images and videos to users.

Traditionally, the compensation technology of OLED displays is typically based on two types of compensation circuits. First, the internal compensation circuit controls the driving voltage of the TFT device with pixel circuits such as 5T1C or 4T0.5C to compensate for the luminance degradation. The internal circuit can compensate for the deviation in the driving voltage of the TFT device. However, when an internal compensation circuit is added, the structural design requirements of the TFT-OLED device become complex, and a highly sophisticated process is required [17]. Moreover, when this internal compensation circuit is utilized, it is difficult to miniaturize the pixels. Therefore, alternative circuit compensation methods are needed for the ultra-minimization of pixels that is necessary to develop high-resolution OLED displays. Second, the external compensation circuit is a mechanism that senses the characteristics of TFT elements inside the panel using sensing circuits from the outside. It then performs a compensation operation in the data voltage application section [18,19]. That is, this circuit is composed of various types of sensing devices. However, the compensation circuit requires additional external sensing circuits, logic circuits, and external memory with a simple pixel structure. In particular, an analog-to-digital converter (ADC) is required for sensing, in addition to memory for the storage of the sensing data. Thus, the cost of development is higher than that of the internal compensation circuit. Therefore, more effective technology is required to design and build a low-cost and high-performance compensation circuit.

We propose a deep learning algorithm that directly compensates for luminance degradation in real time by using a data-driven approach to address the disadvantages of internal and external compensation circuits. Deep learning is a machine learning paradigm that infers information and extracts features from the given data using multiple processing layers. The results of several studies have shown that deep learning facilitates improved performance compared to traditional approaches in a variety of applications that use sensor data [3,20–23]. In this study, the usage time, temperature, average brightness, data voltage deviation of the TFT device, and current supplied from TFT to OLED are used as input data for the training of the proposed deep learning algorithm. In addition, the deviation between the initial luminance of the OLED device and the luminance degradation due to deterioration is used as the target data. As such, the target data is the luminance that is compensated, and this value is obtained by subtracting the degraded luminance value from the initial luminance. When a deep learning algorithm is trained using input data and target data composed of these variables, it performs as a novel circuit that directly estimates the luminance that requires compensation. Ultimately, it is possible to address the limitations of the existing internal and external compensation circuits, such as the complexity of circuit design, high cost, and difficulty of miniaturization. In addition, in the past, when TFT-OLED devices were changed, the compensation circuit had to be redesigned according to the new characteristics. However, the proposed deep learning algorithm can re-learn and reuse the characteristics of the new TFT-OLED device. We evaluated the performance of the model by calculating the deviation between the compensated luminance and the

initial luminance in frames to evaluate the performance of the proposed method and to address the phenomenon problem, which is spread within an error range of 4.56%.

2. DATA SIMULATOR

A data simulator is proposed to obtain the burn-in-related variables of TFT-OLED devices as similar to a typical environment. First, the proposed data simulator uses the specifications of LD420EUN-UHA1 as a Si:H transistor, which is a TFT model. Using the data simulator, it is possible to generate pixel-by-pixel data from 0 to 10,000 h in 100-hour increments from the input video. In addition, it is possible to generate pixel data from OLED displays for low temperature, room temperature, and high temperature from 0°C to 60°C. The data simulator is developed to create data similar to a typical environment by mixing white noise with the generated pixel data. The data generated in this study are used to train the deep learning model in Section 4; the deep learning model is used to examine the correlation between the variables related to the TFT-OLED device that fluctuates in real time and the luminance of the deteriorated OLED device.

Figure 1 shows a block diagram of the data simulator. The input video comprised of various content-specific videos has a total length of 120 min, 30 fps, and a pixel size of 400×300 pixels. The detailed configuration of the input videos of the data simulator is presented in Table 1. Table 2 lists the parameters used in this section.

Table 1: Specifications of input videos.

Contents	Specifications
Content 1 (40 mins)	Documentary, Action, News, Sports
Content 2 (40 mins)	Entertainment, Beauty, Animation, Car review
Content 3 (40 mins)	Game, Cooking, Job introduction, Romance

The order of operation of the data simulator is as follows:

1. First, the data simulator outputs i) the average brightness per pixel ($\bar{B}_p$) and ii) operation time (t_p) from the input video. It also adds iii) a temperature condition (T) between 0°C and 60°C, which affects the deterioration of the TFT and OLED devices.
2. The previously obtained $\bar{B}_p, t_p, T$ variables are used to output iv) the operation time with weights per pixel (t'_p) and v) the degraded TFT data voltage ($V_{d,t'_p=\gamma}$) with the change of time and temperature. White noise is also mixed to create conditions similar to real-world environments.
3. $V_{d,t'_p=\gamma}$ is used for each time and temperature to output vi) the degraded OLED current ($I_{d,t'_p=\gamma}$) of the TFT and to mix the white noise.
4. vii) Degraded OLED luminance ($L_{t'_p=\gamma}$) is observed using $I_{d,t'_p=\gamma}$ for each time and temperature. viii) The initial OLED luminance ($L_{t_p=0}$) is obtained directly from the input video.
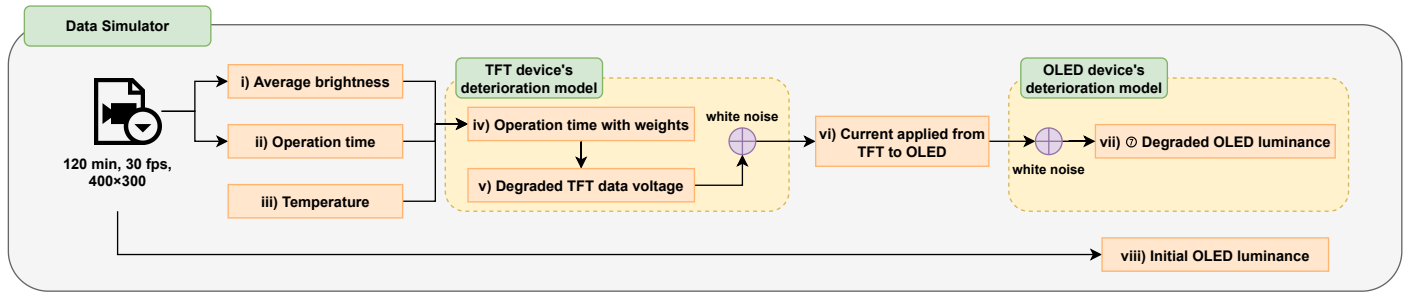
Figure 1. A block diagram of proposed Data Simulator.

Table 2: Nomenclature of paper.

Symbol	Parameter	Symbol	Parameter
F_N	Data of input video	N	Total frame of input video
f	Frame	P	Total pixel
p	Pixel	t	Time
t_p	Operating time per pixel	t'_p	Weighted operating time
B_p	Brightness of per pixel	$\bar{B}_p$	Average brightness per pixel
ϵ_1	Noise of threshold voltage	ϵ_2	Noise of mobility
α_1	Reduction factor of shifting value of threshold voltage	α_2	Reduction factor of threshold voltage
α_3	Reduction factor of mobility	I_{max}	Maximum input current of TFT
L	Length of TFT channel	W	Width of TFT channel
V'_d	Data voltage of TFT that consider noise	$V_{d,t_p=0}$	Initial data voltage of TFT
C_{ox}	Capacitor of TFT unit area	μ	Initial mobility of TFT
V'_{th}	Threshold voltage of TFT that consider noise	V_{DD}	Drain voltage of TFT
T_{limit}	Maximum temperature of TFT performance guarantee	$\triangle V_{shift}$	Shifting value of threshold voltage
$V_{th,t_p=0}$	Initial threshold voltage of TFT	w	Weight factor
n	Gray level of TFT	l	Total gray level range
α	Reduction rate of OLED voltage	T	Temperature
β	Transistor Parameter	C_i	Gate capacitor
W	Channel width		

Algorithm 1 shows the calculation process for the operation time and average brightness of the pixels for each frame from the video data input to the data simulator.

Algorithm 1 Calculation of the operating time per pixel.

Input

   N : total number of frames

  F_N : frame number

   h : height of pixels for frames (300 pixels)

  w : width of pixels for frames (400 pixels)

  B_p : brightness of pth pixel

Output

  t_p : operating time of pth pixel

  $\bar{B}_p$: average brightness of pth pixel

initialization

$p = 0$; $t_p = 0$; $\bar{B}_p = 0$;

while $F_N < N$ **do**

  for $p < (h \times w)$ **do**

    $\bar{B}_p += B_p$;

    if $B_p = 0$ **then**

      $t_p = t_p$; //time is not counted when the pixel does not operate

    else

      $t_p += 1$; //time is counted when the pixel operates

    end

  end

end

$\bar{B}_p = \bar{B}_p / N$;

In particular, the average brightness and operation time of the input video obtained using this algorithm are used in equation (1) to obtain the weighted operation time (t'_p) required for the pixel to emit a specific brightness. Here, ω has a constant value of 0.8 and adjusts the weight to represent the average pixel brightness ($\bar{B}_p$) during the operating time.

$$t'_p \triangleq t_p \left(1 + w\bar{B}_p\right) \tag{1}$$

We also generate white noise to represent the environmental noise that can occur in the OLED display using electronic circuits.

$$\epsilon_1 \sim N(0, \frac{(\max(V_{\text{th}}) + \min(V_{\text{th}}))/2}{100}) \tag{2}$$

$$\epsilon_2 \sim N(0, \frac{(\max(\mu) + \min(\mu))/2}{100}) \tag{3}$$

Next, the threshold voltage shift value (ΔV_{shift}), threshold voltage (V_{th}), and electron mobility (μ) are calculated using the previously determined t'_p and T value as follows.

$$\triangle V_{\text{shift}} \triangleq t'^{\alpha_1}_p \tag{4}$$

$$V_{\text{th}} \triangleq e^{\alpha_2(T - T_{\text{limit}})} + |\triangle V_{\text{shift}}| + \epsilon_1 \tag{5}$$

$$\mu \triangleq e^{-\alpha_3 T} + \epsilon_2 \tag{6}$$

The data voltage ($V_{d,t'_p=\gamma}$) of the TFT is then obtained using V_{th} and μ [24]. Here, V_{DD} is the drain voltage of 4.9V and additive noise, ϵ.

$$V_{d,t'_p=\gamma} \triangleq V_{\text{DD}} - \sqrt{\left(\frac{100}{100-\alpha}\right)\left(\frac{n}{l}\right)\frac{2I_{\max}'}{\mu}C_{ox}\left(\frac{W}{L}\right)} - |V_{\text{th},t'_p=\gamma}| + \epsilon \tag{7}$$

Now, we use V_{th} and $V_{d,t'_p=\gamma}$ to determine the current applied from the TFT to the OLED ($I_{t'_p=\gamma}$) such that.

$$I_{t'_p=\gamma} \triangleq \frac{\beta}{2}(V_{\text{DD}} - V_{d,t'_p=\gamma} - |V_{\text{th}}|), \quad \beta = \mu C_i \frac{W}{L} \tag{8}$$

where $I_{t'_p=\gamma}$ is used to obtain the luminance value ($L_{t'_p=\gamma}$) at a specific time. The following is a mathematical model of the deterioration characteristics of the OLED device, where m_I and η_I have constant values [25].

$$L_{t'_p=\gamma} \triangleq L_0 exp\left\{-\left(\frac{t'_p}{\eta_I\left(\frac{I_0}{I_{t'_p=\gamma}}\right)^\beta}\right)^{m_I}\right\} \tag{9}$$

When the video is served as the input to the data simulator, eight variables associated with the deterioration of the TFT-OLED device are created. Four of the eight variables are used as input data for the deep learning algorithm, and the luminance deviation obtained by subtracting the degraded OLED luminance value from the initial OLED luminance value is used as the target data. In addition, all pixels of the OLED are independently driven; therefore, the correlation between each pixel data generated by the data simulator is not considered. As such, 6,000 independent OLED burn-in data points are generated for each pixel between 0 to 10,000 h in units of 100 h and temperatures between 0°C to 60°C in units of 1°C. The total burn-in datasets are generated 0.12 million (400×300) according to the number of pixels, and 720 million datasets (100×60×400×300) are generated according to time and temperatures for each color; R, G, and B.

3. Data Augmentation

In general, increasing the amount of data improves the performance of deep learning models [26]. We also generate additional data via data augmentation; subsequently, we conduct training using these data together with the existing data. Furthermore, natural data in the real world has noise due to various conditions such as temperature, humidity, and initial tolerance. This means that it is necessary to reflect this noise and generate data similar to natural data as much as possible. The bootstrap method is an approach for increasing the training data using random sampling. Figure 2 shows a block diagram of the proposed data augmentation algorithm based on the bootstrap method. First, 60 million samples are drawn six times using random sampling from 720 million pixel data generated through a data simulator. The sample extracted in this method is called a bootstrap sample, and the mean and standard deviation of each bootstrap sample are calculated. Then, 60 million random number data are generated based on the calculated mean and standard deviation in order to obtain noise that follows the Gaussian statistical distribution of the bootstrap sample data. The generated random number data is multiplied by a constant weight of 0.01 to reduce information loss of the original data that may occur when noise is applied. Finally, 60 million bootstrap sample data is multiplied by each random number data to generate new data. Since this method generates noise through the distribution of each bootstrap sample, it can generate noise similar to the distribution of the original image. Consequently, by applying the 720 million pixel data generated in the data simulator, 360 million training data with independent characteristics are additionally generated for each R, G, and B color.
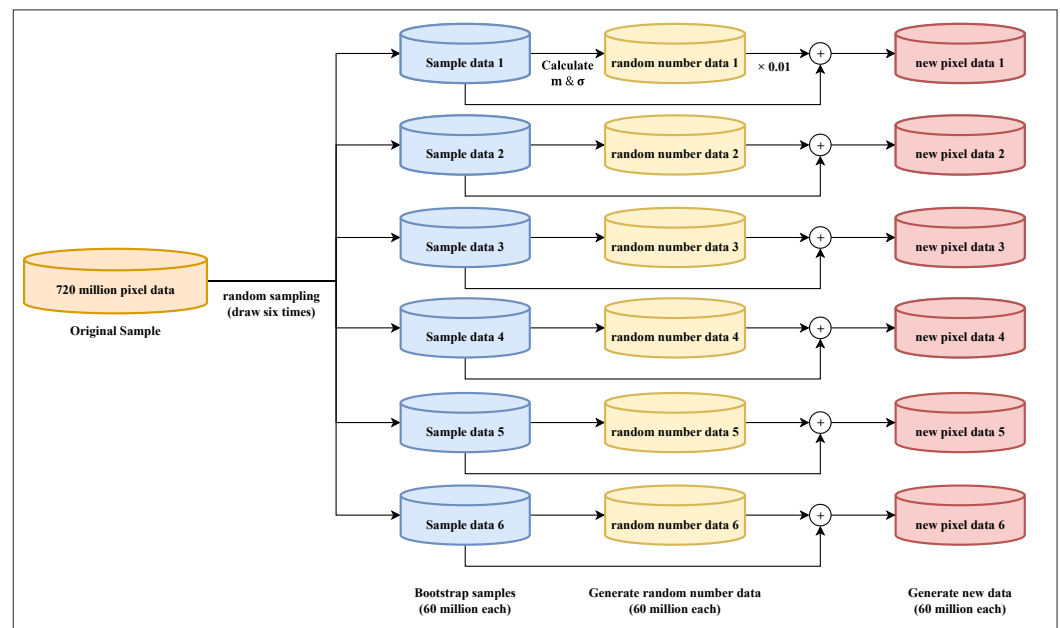
Figure 2. A block diagram of the bootstrap method.

4. Deep Learning Model

4.1. Data Configuration

The data used in the deep learning model consists of four features (t'_p, T, $V_{d,t'_p=\gamma}$, $I_{d,t'_p=\gamma}$), consisting of vector forms with (1, 4) dimensions. The target data is one of the features, that is, the deviation luminance ($L_{t_p=0}$ - $L_{t'_p=\gamma}$) that requires compensation. The total training data consists of 1.08 billion input data and target data pairs for each R, G, and B color. Figure 3 shows the structure of the proposed entire deep learning model, which is trained to estimate the deviation luminance ($\hat{L}_{t'_p=\gamma}$), which requires compensation.
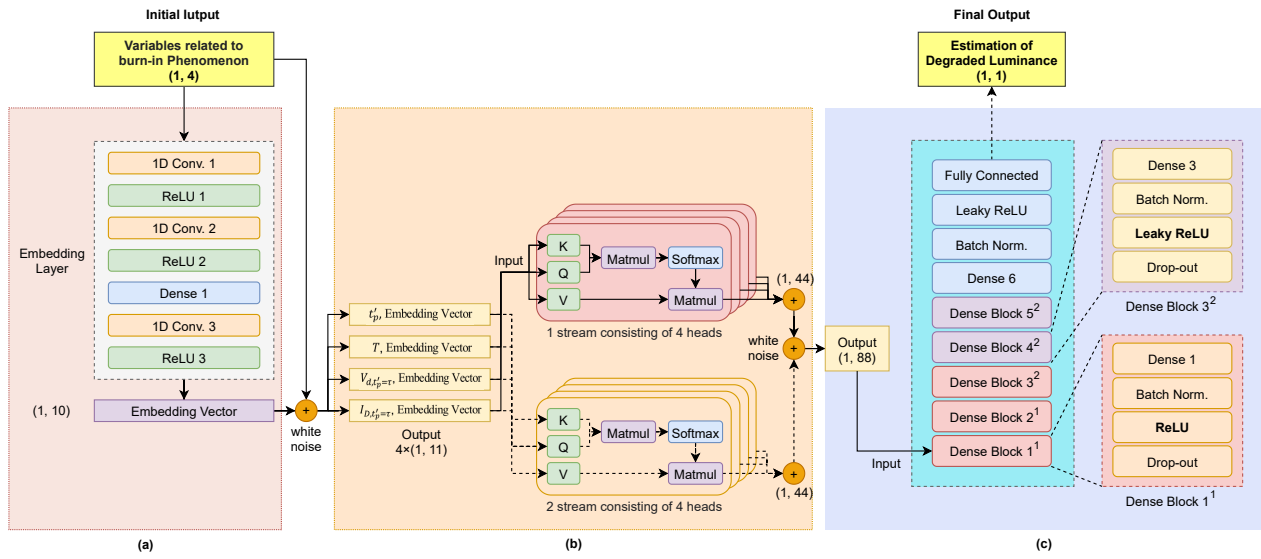
Figure 3. Overview of the whole model: (a) deep feature generation; (b) multi-stream self-attention; (c) deep neural network.

4.2. Deep Feature Generation

Feature generation is also known as feature construction, feature extraction or feature engineering. It is used to create new features from one or several features [27]. The implementation of this approach as a deep learning technique is called deep feature generation. Thus, in addition to the features generated using the data simulator, the features associated with OLED deterioration are also generated during the training process of the deep learning model to make them similar to the OLED burn-in data. In this study, we propose a deep feature generation algorithm composed of a 1D convolutional neural network (1D CNN), deep neural network (DNN), and rectified linear units (ReLU) [28], which are nonlinear functions, as shown in Figure 4. Using this algorithm, new features (embedding vectors) are also extracted using the existing input data with dimensions of (1, 4). First, 1D CNNs are available for 1D signal variables that cannot use 2D CNNs; the computational burden is lower than that of 2D CNNs, making them suitable for real-time processing and low-cost hardware implementations [29]. In addition, the DNN extracts information on the correlation between features by completely connecting the outputs of the 1D CNN. This DNN facilitates a nonlinear combination of input features and feature extraction is performed automatically. In the final output of this deep feature generation algorithm, 10 new features are generated with dimensions (1, 10). White noise is mixed to represent the noise in the OLED display circuit environment. Subsequently, one of the four original features is selected and concatenated to the new features, resulting in a new form of data with a higher dimension (1, 11) than the original dimension (1, 4).
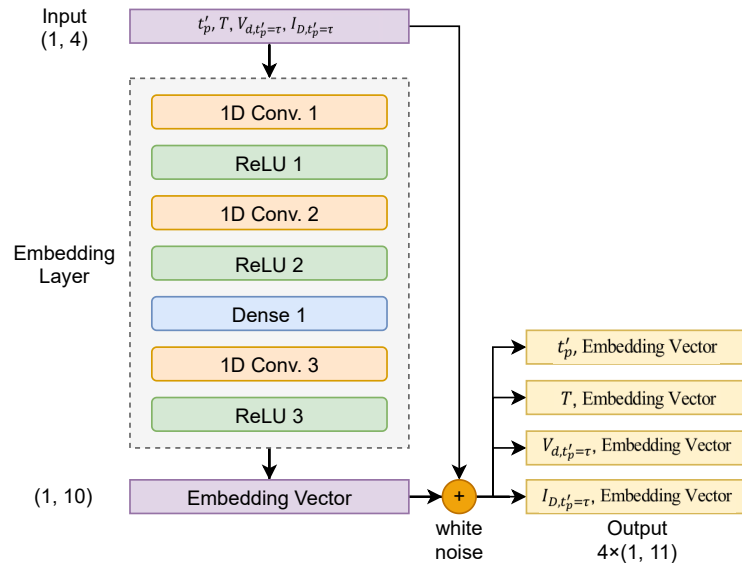
Figure 4. Overview of the proposed deep feature generation model.

4.3. Multi-stream Self-attention

Multi-stream self-attention [30] has already been applied to the field of speech recognition to show state-of-the-art. Based on the idea of this algorithm, we propose a modified multi-stream self-attention that is optimized for learning the outputs of deep feature generation. The proposed multi-stream self-attention consists of two multi-head self-attention layers [31] each of which consists of four self-attention layers, as shown in Figure 5. The operation process of this algorithm proceeds in the following order. First, the multi-stream self-attention improves the performance of deep learning algorithms with ensemble-like effects. Second, the multi-head self-attention corresponding to each stream is trained by increasing the weight of the most important feature to effectively compensate for the degraded luminance among the input features. Similarly, less important features are trained such that the weight is reduced; that is, when four input data with dimensions (1, 11) are input to each head, an extraction process is performed that represents the importance of each feature by adjusting the weight value to focus on the most important of the 11 features. Third, given that the output of the multi-head self-attention maintains the dimension of the input data, the data with the (1, 44) dimension is output by concatenating four outputs of each head. Finally, the multi-stream self-attention outputs data with dimensions (1, 88) as two outputs.
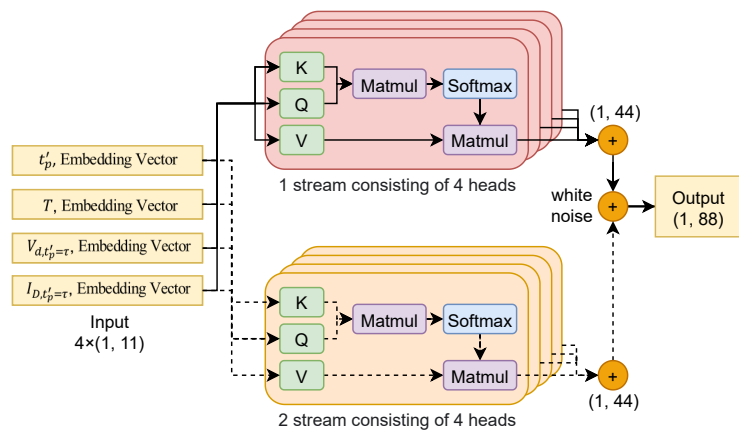
Figure 5. Overview of the multi-head self-attention model.

4.4. DNN

Recently, the DNN [32] has been successfully utilized in applications such as image processing, automatic speech recording, and natural language processing. As shown in Figure 6, the proposed algorithm consists of *DenseBlock*^{1}, *DenseBlock*^{2}, a single dense layer, and a fully connected layer. *DenseBlock*^{1} comprises of a single dense layer, batch normalization layer, ReLU, and dropout. *DenseBlock*^{2} is a nonlinear function of *DenseBlock*^{1}, ReLU, replaced by Leaky-ReLU, which is proposed to solve the dying ReLU phenomenon. This DNN algorithm is trained to identify nonlinear relationships between input data and target data by recognizing specific patterns when data with dimensions (1, 88) are inputted. For the final output, we obtain the value of the dimension (1, 1) of luminance ($\hat{L}_{t'_p = \gamma}$) that requires compensation.
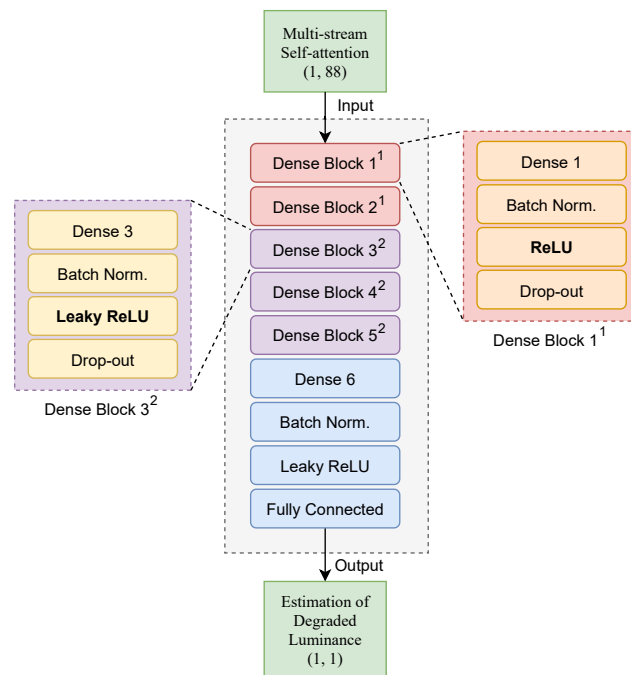
Figure 6. Overview of the proposed deep neural network model.

5. Experimental Environment and Result

5.1. Datasets

In our experiments, we used the blue pixel data, which has the largest power consumption and a much faster degradation rate compared to red and green pixel data [33]. Therefore, a deep learning based compensation algorithm was trained and evaluated using 1.08 billion datasets of blue pixel generated using data simulators and data augmentation. The compositions of the datasets, divided into training data and test data, are shown in Table 3. Figure 7 shows respectively the power consumption and the luminance degradation rate for the blue, red and green pixel.

Table 3: The composition of the datasets.

Datasets	Train / Test	Total
OLED pixel (Blue)	9.72 billion / 1.08 billion	10.8 billion
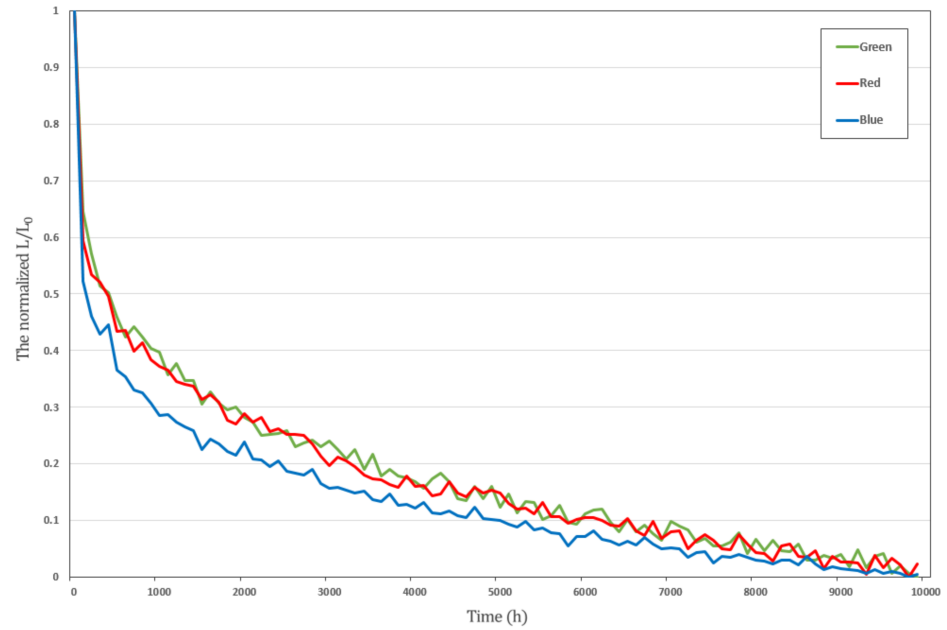
Figure 7. Luminance degradation rate for the normalized blue, red and green pixel data.

5.2. Experimental Setup

All experiments in this study were conducted using TensorFlow in Python library. Batch normalization [34] was applied to the DNN, and the Adam optimizer [35] with a learning rate of 0.001 was used for training a deep learning algorithm. In addition, the batch size used in the training process was 6,000, and all parts of the algorithm were jointly optimized with the mean absolute percentage error (MAPE) used as a loss function in the following. The algorithm was trained for 50 epochs; if the validation loss did not improve within three epochs, an early pause was applied. In addition, the accuracy of the algorithm was calculated using MAPE, as shown below.

$$\text{MAPE} = \frac{1}{NP} \sum_{f=1}^{N} \sum_{p=1}^{P} \left| \frac{L_{t_p=0} - \hat{L}_{t'_p=\gamma}}{L_{t_p=0}} \right| \tag{10}$$

$$\text{Accuracy} = 100\left(1 - \frac{1}{NP} \sum_{f=1}^{N} \sum_{p=1}^{P} \left| \frac{L_{t_p=0} - \hat{L}_{t'_p=\gamma}}{L_{t_p=0}} \right|\right)(\%) \tag{11}$$

5.3. Results Analysis

As shown in Table 4, in the case of deep feature generation, experiments were conducted with three models; experiment 2 demonstrated the best accuracy at 91.62%. As depicted in Table 5, based on the testing of the 1-stream self-attention and 2-stream self-attention algorithms. Experiment 2 showed an accuracy of 92.19%. When using three or more streams, there was a tendency to overfit as the number of streams increased.

Table 5: Accuracy (in %) comparison of the proposed models with Multi-stream Self-attention [30].

Experimental Details	Experiment 1	Experiment 2
	1-Stream Self-attention	2-Stream Self-attention
Accuracy	90.75%	**92.19%**

In Table 6, experiments were conducted by changing the number of DNN layers in deep

Table 4: Accuracy (in %) comparison of the proposed models composed of different hyper-parameters with Deep Feature Generation (layers, kernel, filter size, and units).

Experimental Details	Experiment 1		Experiment 2		Experiment 3	
	Layers	**Kernel Filter Size Units**	**Layers**	**Kernel Filter Size Units**	**Layers**	**Kernel, Filter Size Units**
	1D Conv 1	1×4 @32	1D Conv 1	1×4 @32	1D Conv 1	1×4 @32
	1D Conv 2	1×32 @16	1D Conv 2	1×32 @16	Dense 1	32
	Dense 1	16	Dense 1	16	1D Conv 2	1×32 @16
			1D Conv 3	1×16 @10	Dense 2	16
					1D Conv 3	1×16 @10
Accuracy	90.28%		**91.62%**		91.45%	

Table 6: Accuracy (in %) comparison of proposed models with different numbers of Deep Neural Network's layers.

Experimental Details	Experiment 1		Experiment 2		Experiment 3	
	Layer number	**Units**	**Layer number**	**Units**	**Layer number**	**Units**
	Dense layer 1	64	Dense layer 1	64	Dense layer 1	64
	Dense layer 2	64	Dense layer 2	64	Dense layer 2	64
	Dense layer 3	64	Dense layer 3	64	Dense layer 3	64
	Dense layer 4	64	Dense layer 4	64	Dense layer 4	64
			Dense layer 5	64	Dense layer 5	64
					Dense layer 6	64
Accuracy	89.94%		91.22%		**93.31%**	

neural networks; experiment 3 demonstrated an accuracy of 93.31%, which indicates that six layers are suitable.

Also, Table 7 shows the experimental results obtained by adjusting the number of units in each layer of the DNN algorithm. The DNN algorithm used six layers, as obtained from the experimental results in Table 6. As a result, experiment 4 with a bottleneck structure demonstrated an accuracy of 95.44%.

Therefore, as shown in Tables 4, 5, 6, and 7, the final performance of the deep learning based compensation algorithm is the best accuracy of 95.44%. Figure 8 compares the initial display image, the image in which luminance degradation occurred, and the image in which the degraded luminance was compensated.

(a)   (b)   (c)
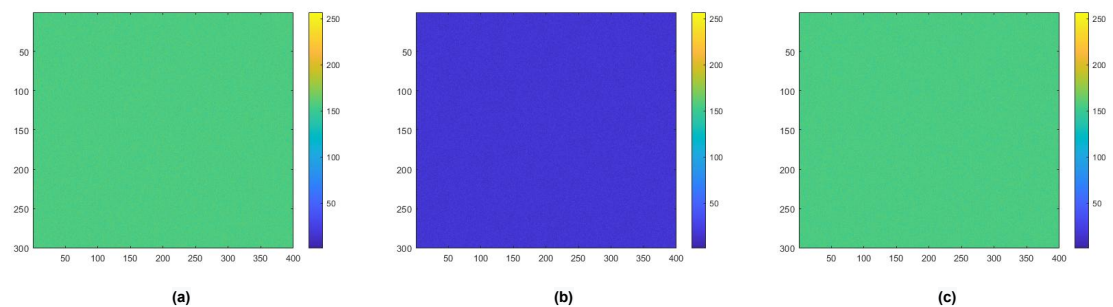
Figure 8. The image of OLED Display (400×300) according to the number of pixels: (a) The initial display image; (b) The image in which luminance degradation occurred; (c) the image when degraded luminance was compensated.

6. Conclusion

In this study, we proposed the deep learning algorithm to address the burn-in phenomenon of OLED displays by using deep learning technology. This algorithm can replace physical circuit-based internal and external compensation circuits that compensate after sensing the degraded TFT data voltage or TFT-OLED current and calculating the luminance degradation value of OLED display due to the deterioration of OLED devices. This means that the proposed compensation method based on deep learning algorithm doesn't need to add internal and external compensation circuits for calculating the luminance degradation. In particular, even if a new TFT-OLED device is developed, the significant advantage is that only the deep learning algorithm can be re-learned according to the parameters of the device and reused without the need to change the physical circuit. Furthermore, if OLED display is combined with cloud service, deep learning algorithm can be easily improved remotely. In the future, we will supplement the data simulator based on real data and augment the burn-in data to strengthen the deep learning based compensation algorithm.

Author Contributions: Conceptualization, Park, S., Park, K. and Chang, J. -H.; methodology, Park, S. and Park, K.; software, Park, S. and Park, K.; validation, Park, S.; writing, original draft preparation, Park, S.; writing, review and editing, Chang, J. -H.; supervision, Chang, J. -H.; project administration, Chang, J. -H.; funding acquisition, Chang, J. -H.

Conflicts of Interest: The authors declare no conflict of interest.

References

1. Kang, S.–. OLED power control algorithm using optimal mapping curve determination. *J. Display Technol* **2016**, *12*, pp. 1278-1282.
2. Jung, H.; Kim, Y.; Chen, C.; Kanicki, J. A-IGZO TFT based pixel circuits for AM-OLED displays. *Proc. SID Tech. Dig* **2012**, pp. 1097-1100.
3. Wang, C.; Hu, Z.; He, X.; Liao, C.; Zhang, S. One gate diode-connected dual-gate a-IGZO TFT driven pixel circuit for active matrix organic light-emitting diode displays. *IEEE Trans. Electron Devices* **2016**, *63*, pp. 3800-3803.
4. In, H.-J.; Kwon, O.-K. External compensation of nonuniform electrical characteristics of thin-film transistors and degradation of OLED devices in AMOLED displays. *IEEE Electron Device Lett.* **2009**, *30*, pp. 377-379.

Table 7: Accuracy (in %) comparison of the proposed models with different numbers of units of Deep Neural Network's layers.

	Layer number	Experiment 1	Experiment 2	Experiment 3	Experiment 4	Experiment 5
		Units				
Experimental Details	Dense layer 1	64	128	256	256	256
	Dense layer 2	64	128	256	128	128
	Dense layer 3	64	128	256	128	128
	Dense layer 4	64	128	256	256	256
	Dense layer 5	64	128	256	128	128
	Dense layer 6	64	128	256	64	128
Accuracy		92.58%	93.35%	93.76%	**95.44%**	95.10%

5. Lee, K.–Y.; Chao, Y.-P.; Chen, W.-D. A new compensation method for emission degradation in an AMOLED display via an external algorithm, new pixel circuit, and models of prior measurements. *J. Display Techno.* **2014**, *10*, pp. 189-197.

6. Xia, S. C.; Kwong, R. C.; Adamovich, V. I.; Weaver, M. S.; Brown, J. J. OLED device operational lifetime: Insights and challenges. in *Proc. 45th Annu. IEEE Int. Rel. Phys. Symp.* **2007**, pp. 253–257.

7. Zhou, X. et al. Real-time observation of temperature rise and thermal breakdown processes in organic LEDs using an IR imaging and analysis system. *Adv. Mater.* **2000**, vol. 12, no. 4, pp. 265–269.

8. Kundrata, J.; Baric, A. Electrical and thermal analysis of an OLED module. in Proc. Comsol Conf., 2012.

9. Kim, H.; Shin, H.; Park, J.; Choi, Y.; Park, J. Statistical modeling and reliability prediction for transient luminance degradation of flexible OLEDs. *2018 IEEE International Reliability Physics Symposium (IRPS)* **2018**, pp. 3C.7-1-3C.7-6.

10. Mian Dong; Choi, Y. K.; Zhong, L. Power modeling of graphical user interfaces on OLED displays. 2009 46th ACM/IEEE Design Automation Conference, 2009, pp. 652-657.

11. Hadizadeh, H. Energy-Efficient Images. in *IEEE Transactions on Image Processing*, vol. 26, no. 6, pp. 2882-2891, June **2017**, doi: 10.1109/TIP.2017.2690523.

12. Chang, T.; Xu, S. S. Real-time quality-on-demand energy-saving schemes for OLED-based displays. *2013 IEEE International Symposium on Industrial Electronics* **2013**, pp. 1-5, doi: 10.1109/ISIE.2013.6563813.

13. Scholz, S.; Kondakov, D.; Lussem, B.; Leo, K. Degradation mechanisms and reactions in organic light-emitting devices. *Chemical reviews* **2015**, *115*, pp. 8449-5803.

14. Langlois, E.; Wang, D.; Shen, J. Degradation mechanisms in organic light emitting diodes. *Synth. Metals* **2000**, *111*, pp. 233-236.

15. Schmidbauer, S.; Hohenleutner, A.; Konig, B. Chemical Degradation in Organic Light-Emitting Devices: Mechanisms and Implications for the Design of New Materials. *Adv. Mater.* **2013**, *25*, pp. 2114-2129.

16. Fery, C.; Racine, B.; Vaufrey, D.; Doyeux, H.; Cina, S. Physical mechanism responsible for the stretched exponential decay behavior of aging organic light-emitting diodes. *Appl. Phys. Lett.* **2005**, *87*, pp. 213502-213503.

17. Lee, K.-Y.; Hsu, Y.-P.; Chao, C.-P. A new 4T0.C AMOLED pixel circuit with reverse bias to alleviate OLED degradation. *IEEE Electorn Device Lett.* **2012**, *33*, pp. 1024-1026.

18. Lin, C.-L.; Chen, Y.-C. A novel LTPS-TFT pixel circuit compensating for TFT threshold-voltage shift and OLED degradation for AMOLED. *IEEE Electron Device Lett.* **2007**, *28*, pp. 129-131.

19. Lee, K.-Y.; Chao, C.-P. A new AMOLED pixel circuit with pulsed drive and reverse bias to alleviate OLED degradation. *IEEE Electron Device Lett.* **2012**, *59*, pp. 1123-1130.

20. Zeng, M.; Nguyen, Le T.; Yu, Bo.; Mengshoel, Ole J.; Zhu, J.; Wu, P.; Zhang, J. Convolutional neural networks for human activity recognition using mobile sensors. In Proc. 2014 6th Int. Conf. Mobile Comput., Appl. Services, pp. 197–205, Nov. 2014.

21. Rav'ı, D.; Wong, C.; Lo, B.; Yang, G. -Z. A Deep Learning Approach to on-Node Sensor Data Analytics for Mobile or Wearable Devices. *IEEE Journal of Biomedical and Health Informatics* **2017**, *21*.

22. Krizhevsky, A.; Sutskever, I.; Hinton, G. E. Imagenet classification with deep convolutional neural networks. *Proc. Adv. Neural Inf. Process. Syst. 25* **2012**, pp. 1097–1105.

23. Psuj, G. Degradation mechanisms in organic light emitting diodes. *Sensors 18 (2): 292* **2018**, https://doi.org/10.3390/s18010292

24. In, H.-J.; Kwon, O.-K. External Compensation of Non-uniform Electrical Characteristics of Thin-Film Transistors and Degradation of OLED Devices in AMOLED Displays. *IEEE Electron Device Letters* **2009**, *30*.

25. Zhang, J.; Li, W.; Cheng, G.; Chen, X.; Wu, H.; Shen, H. Life prediction of OLED for constant-stress accelerated degradation tests using luminance decaying model. *Appl. Phys. Lett.* **2014**, *154*, pp. 491-495.

26. Taylor, L.; Nitschke, G. Improving Deep Learning using Generic Data Augmentation. *arXiv:1708.06020v1* **2017**.

27. Bosch, S. V. D. Automatic feature generation and selection in predictive analytics solutions. Master's thesis, Faculty of Science, Radboud University, vol. 3, no. 1, p. 3.1, 2017.

28. Agarap, F. Deep learning using rectified linear units (relu). *arXiv preprint arXiv:1803.08375* **2018**.

29. Kiranyaz, S. 1-D Convolutional Neural Networks for Signal Processing Applications. In ICASSP 2019 – 2019 IEEE International Conference on Acoustics, Speech and Signal Processing (ICASSP), pp. 8360–8364, 2019.

30. Han, K. J.; Prieto, R. State-of-the-art speech recognitions using multi-stream self-attention with dilated 1D convolutions. *arXiv:1910.00716v1* **2019**.

31. Vaswani, A.; Shazeer, N.; Parmar, N.; Uszkoreit, J.; Jones, L.; Gomez, A. N.; Kaiser, Ł.; Polosukhin, I. Attention is all you need. *Advances in Neural Information Processing Systems* **2017**, pp. 5998–6008.

32. Heaton, J.; Goodfellow, I.; Bengio, Y.; Courville, A. Deep learning. *Genet Program Evolvable Mach.* **2018**, https://doi.org/10.1007/s10710-017-9314-z.

33. Yeh, C.-H. Visual-Attention-Based Pixel Dimming Technique for OLED Displays of Mobile Devices. *IEEE Transactions on industrial electronics* **2019**, *66*.

34. Ioffe, S.; Szegedy, C. Batch normalization: Accelerating deep network training by reducing internal covariate shift. Available online: https://arxiv.org/pdf/1502.03167.pdf (accessed on 19 September 2019).

35. Kingma, D. P.; Ba, J. Adam: A method for stochastic optimization. Available online: https://arxiv.org/pdf/1412.6980.pdf (accessed on 19 September 2019).